High-temperature superconductivity in a topological insulator

Parisa Zareapour[1*], Alex Hayat[1,2*], Shu Yang F. Zhao[1], Anjan Reijnders[1], Mikhail Kreshchuk[1], Achint Jain[1], Daniel C. Kwok[3], Nara Lee[3], Sang-Wook Cheong[3], Zhijun Xu[4], Alina Yang[4], G. D. Gu[4], and Kenneth S. Burch[1]

[1]*Department of Physics and Institute for Optical Sciences, University of Toronto, 60 St. George Street, Toronto ON, M5S 1A7, Canada*

[2]*Centre for Quantum Information and Quantum Control University of Toronto, 60 St. George Street, Toronto ON, M5S 1A7, Canada*

[3]*Rutgers Center for Emergent Materials and Department of Physics and Astronomy, Rutgers University, 136 Frelinghuysen Road, Piscataway, New Jersey 08854, USA*

[4]*CMP&MS Department, Brookhaven National Laboratory, Upton, New York 11973, USA*

Producing new effects through the combination of different materials has a long history in science and technology. One of the most intriguing recent ideas is the emergence of Majorana fermions when a topological insulator is placed in proximity with a superconductor. Towards this goal, we produced high-temperature superconductivity in the topological insulator Bi_2Se_3 via the proximity to $Bi_2Sr_2CaCu_2O_{8+\delta}$. This was achieved through a new mechanical bonding technique enabling the fabrication of high-quality junctions between novel materials, unobtainable by conventional approaches. The results presented here open new directions for fundamental studies in condensed matter physics and enable a wide range of applications in spintronics and quantum computing.

---

[*] These authors contributed equally to this work.

Novel phenomena in matter are often obtained by spontaneous symmetry breaking. Therefore, much of modern solid-state physics research has focused on tuning materials to new regimes, such as efforts to study non-Fermi liquid states *(1),* high-temperature superconductivity *(2),* and Bose-Einstein condensation *(3).* Lately, a different paradigm for finding new properties in the solid state has emerged, namely through the sudden change in topological invariants rather than the breaking of symmetries. These topological phases of matter have been proposed *(4,5,6)* and demonstrated experimentally *(7,8)* to exist at the surface of some materials with strong spin-orbit coupling. These topological insulators (TI) have topologically-protected surface states predicted to reveal various physical properties including axion electrodynamics *(9),* as well as practical applications including dissipationless spin currents *(10)* crucial to spintronics *(11).*

Perhaps most exciting is the proposal to produce the elusive Majorana fermion by combining both concepts - the broken gauge symmetry of a superconductor with the sudden change in topological invariants at the surface of a TI *(12).* If obtained, the Majorana fermion would usher in a new era for particle and condensed-matter physics, as well as enable novel quantum technologies such as fault-tolerant topological quantum computing *(13,14).* The original proposal of proximity-induced superconductivity in an undoped bulk TI put forward by Fu and Kane has not been demonstrated experimentally yet. The proposal has nonetheless reinvigorated the long-studied problem of the proximity effect *(15),* where superconducting and normal materials are affected by being connected with one another. This effect allows combining different properties of the materials that do not coexist in each individual material, e.g. quasi-relativistic dispersion

in graphene and superconductivity *(16).* Proximity provides a powerful resource of inducing superconductivity locally in any material, and it has been employed recently for realization of new optoelectronic devices *(17).* Most of the proximity-based experiments, however, have been performed with low critical temperature (T_c) superconductors, whereas inducing superconductivity at higher temperatures with high-T_c materials *(18)* can enable future realizations of more practical hybrid superconductor based devices.

Here we present the first experimental demonstration of proximity-induced high-T_c superconductivity in a TI. The effect is achieved by a newly-developed method of mechanically-bonded planar junctions, with a focus on $Bi_2Sr_2CaCu_2O_{8+\delta}$ (Bi-2212) and Bi_2Se_3. We characterize the induced superconducting gap in Bi_2Se_3 by current-voltage and differential conductance measurements, studying the spectra of Andreev scattering - a process where an incident electron (hole) creates a Cooper pair in the superconductor with the reflection of a hole (electron) resulting in an excess current *(19)*. The Bi-2212/Bi_2Se_3 Andreev spectra exhibit both: the proximity-induced superconducting gap within Bi_2Se_3 and the Bi-2212 gap reduced by proximity. The utilization of double-gap Andreev scattering spectra to characterize the proximity effect at superconducting-normal (S-N) interfaces is well established in low-Tc superconductors in contact with normal metals (*20*) or semiconductors *(21)*. Our results show that the induced superconductivity in Bi_2Se_3 persists up to at least 85K – a temperature an order of magnitude higher than any previous observations. Indeed, low-temperature superconductivity has been observed recently in TI with very high levels of Cu doping *(22,23,24),* and in nanostructures with low-T_c superconductor contacts made using complicated fabrication methods *(25,26)*.

We have developed a simple mechanical bonding technique enabling implementation of practical hybrid TI/high-T_c devices. High-quality bulk Bi_2Se_3 and optimally doped Bi-2212 crystals, grown by the floating-zone method were cleaved resulting in atomically flat surfaces over large areas, and were subsequently mechanically-bonded (Fig. 1) in a dry atmosphere. These low-resistance tunnel junctions *(27)* where then probed via tunneling spectroscopy measurements including current and differential conductance versus voltage (Fig. 1). The carrier density of Bi_2Se_3 was determined to be $1.6\times10^{19}cm^{-3}$ *(27)* by far infrared (FIR) spectroscopy (Fig. 1 B). The tunneling spectroscopy experiments were performed using four-point probe measurements in a liquid He flow cryostat at different temperatures ranging from 295K to 4.5K. Our mechanically-bonded tunnel junction method was also verified to perform successfully on Bi-2212/graphite junctions, resulting in typical S-N tunneling spectra *(27).*

The first experiments were performed on low-resistance Bi-2212/Bi_2Se_3 junctions with current along the c-axis. DC voltage versus current (I-V) characteristics (Fig 2A) reveal excess current below the Bi-2212 T_C ~85K, as predicted by the Blonder-Tinkham-Klapwijk (BTK) formalism for very low barrier S-N interfaces *(19).* The observed excess current is a manifestation of Andreev scattering - the key mechanism for the superconducting proximity effect, *(28)* suggesting the existence of a proximity-induced superconducting region at the Bi-2212/Bi_2Se_3 interface. Just below T_c the excess current I_e reaches the maximal value at nearly twice that of the normal-normal (N-N) interface (measured for $T > T_C$) due to the current carried by Cooper pairs when Andreev reflection occurs. At lower temperatures, the excess current is reduced, and the spectrum exhibits

additional features. A different measurement - AC differential conductance below T_c $[dI/dV]_S$, divided by the normal state conductance $[dI/dV]_N$ measured at 105K, with ~8mV resolution, confirms the DC I-V measurement, demonstrating the zero-bias conductance peak due to Andreev scattering below T_C (Fig. 2 B). At lower temperatures (around 60K), reduction of higher-bias current was observed, and at the same temperatures additional higher-bias features appeared in the differential conductance measurement. These features result from the gap reduction in Bi-2212 and the induced gap in Bi_2Se_3. However, the detailed spectrum structure of these features could be studied only at lower temperatures.

To demonstrate the spectral features more clearly, we performed both DC and AC measurements at lower temperatures – well below T_c. DC I-V characteristics of the junction (Fig. 2 C) show excess current at lower voltages up to about 13mV with a correspondingly smaller value I_S ~ 2.7μA. However, two additional step-like features appear near 27mV and 45mV. These features are confirmed by an AC differential conductance measurement (Fig. 2 D), showing a wide conductance feature centered at zero bias between ±13meV, and peaks at ±27mV and ±45mV, in good quantitative agreement with the DC measurement (Fig. 2 C inset). As discussed below, this conductance spectrum is a clear signature of a proximity-induced superconducting region in the Bi_2Se_3.

When proximity effect occurs (Fig. 3 A (I)), the superconducting gap extends into the normal region (Δ_i) such that near the interface it is reduced from the intrinsic value (Δ_0) to a smaller one (Δ_r). Generally, the superconducting gap is position-dependent along the axis normal to the interface plane, $\Delta(x)$, and Andreev scattering probability is

finite in the whole proximity region. However, the scattering can be divided into two main energy ranges: electrons (holes) with energy $|E| < \Delta_i$ will be mainly Andreev reflected inside the induced superconducting region of the normal material, whereas electrons (holes) with $\Delta_i < |E| < \Delta_r$ will continue to the S-N interface and Andreev-reflect mainly inside the superconductor near the interface. Thus, conductance spectrum taken on an interface exhibiting the proximity effect will show Andreev scattering features corresponding to both gaps *(20, 21).* In our experiment, therefore, the central conductance peak is a manifestation of Andreev reflection from the normal region to the proximity-induced superconducting region of Bi_2Se_3 with a gap Δ_i ~13meV. The reduced gap in Bi-2212 due to the proximity effect appears as a conductance peak at Δ_r ~27meV. The change in the zero bias conductance at T_c is an additional manifestation of the Andreev scattering in Bi_2Se_3. Indeed, just below T_c the zero-bias conductance increases to nearly twice its value above T_c (Fig. 3 B). This temperature dependence as well as the spectral shape of the conductance at various temperatures completely rules out any possible heating related effects.

Moreover, a non-uniform junction can have areas with no proximity effect (Fig. 3 A – (II)). These areas will exhibit Andreev scattering with the intrinsic gap of the superconductor, appearing in our experiment as additional peaks at Δ_0 ~ 45mV. The height of the Bi_2Se_3 Andreev zero-bias conductance feature is nearly twice the normal conductance value due to the Cooper pair contribution (Fig. 2 D), whereas the width is determined by the induced superconducting gap, $2\Delta_i$. The width of the Andreev feature is also manifested in the excess current up to a negative bias Δ_i in the DC I-V

characteristic (Fig. 2 C) - nearly twice as high as the current in the normal state (Fig. 2 A). The probability of Andreev scattering inside the Bi-2212 is reduced by the scattering in Bi_2Se_3, resulting in slightly smaller contribution to the conductance at Δ_r.

For the quantitative theoretical modeling of the effect, the c-axis Bi-2212/Bi_2Se_3 tunneling spectra were calculated using an extension of the BTK formalism developed by Kashiwaya and Tanaka for anisotropic superconductors *(29)*. In this formalism the quasiparticles in a superconductor are described by a two-component wavefunction $\Psi(r)=\begin{bmatrix} f(r) \\ g(r) \end{bmatrix}$ corresponding to the electron and hole parts, using Bogoliubov–de Gennes equations:

$$\begin{aligned} i\hbar\frac{\partial}{\partial t}f(r,t) &= \left[-\frac{\hbar^2}{2m}\nabla^2-\mu(r)+V(r)\right]f(r,t)+\Delta(r)\,g(r,t) \\ -i\hbar\frac{\partial}{\partial t}g(r,t) &= \left[-\frac{\hbar^2}{2m}\nabla^2-\mu(r)+V(r)\right]g(r,t)-\Delta(r)\,f(r,t) \end{aligned} \tag{1}$$

where m is the electron and hole mass, $\mu(r)$ is the chemical potential, $V(r)=H\delta(r)$ is the delta-function barrier potential with the strength determined by H, and $\Delta(r)$ is the pairing potential (the superconducting gap). In proximity, the gap is reduced in the superconductor and increased in the normal material (Fig. 3 A (I)), so that the spatial dependence can be described by *(21)*:

$$\Delta(x)=\frac{\Delta_0}{1+e^{(x+a_N)/\xi_N}}\Theta(x)+\frac{\Delta_0}{1+e^{(x-a_S)/\xi_S}}\Theta(-x) \tag{2}$$

where $\Theta(x)$ is a step function, ξ_N (ξ_S) is the normal material (superconductor) coherence length, a_N determines the induced gap in the normal region, and a_S determines the gap reduction in the superconductor. In the vicinity of the interface, the

reduced superconducting gap can be approximated by $\Delta_r \approx \Delta_0 \Big/ \left(1+e^{-a_S/\xi_S}\right)$ and the induced gap in the normal region is $\Delta_i \approx \Delta_0 \Big/ \left(1+e^{a_N/\xi_N}\right)$. Andreev scattering in the proximity region can be modeled therefore by two successive scatterings from two interfaces: scattering within Bi_2Se_3 with the induced gap Δ_i followed by scattering within Bi-2122 with the reduced gap Δ_r. The calculated spectra with the modified gaps as fit parameters show good agreement with the experimental conductance measurements (Fig. 3 D).

To further verify that the Andreev scattering is due to the proximity induced superconductivity in Bi_2Se_3, and dismiss any possible processes occurring in the Bi-2212 alone, the Bi-2212/Bi_2Se_3 junction barrier was increased mechanically. As expected, differential conductance measurement performed on the high-resistance junction revealed only spectra typical of a c-axis tunneling measurement on Bi-2212 *(30),* indicating the lack of a proximity effect. Specifically, the superconducting gap of Bi-2212 was observed, however no Andreev peak appeared at the Bi-2212 reduced gap Δ_r, and no conductance features corresponding to proximity-induced gap in the Bi_2Se_3 (Fig. 3 C). The differential conductance spectrum for the high-resistance junction showed the superconducting gap of Bi-2212 Δ_0, and its temperature dependence agrees with the values from the low-resistance junction measurement (Fig. 3 B inset), confirming the origin of the conductance peaks.

Our results present clear evidence of proximity-induced high-T_c superconductivity in the TI Bi_2Se_3. We achieved this via our newly-developed technique of mechanically-bonded junctions, and confirmed it by various experiments. Specifically,

below T_c we observe Andreev features corresponding to a reduced gap of Bi-2212 appearing concurrently with an induced gap in Bi_2Se_3. The disappearance of these features in the same junctions when the barrier is increased confirms that proximity effect is the origin of these features. The proximity-induced Bi_2Se_3 superconductivity is demonstrated at temperatures at least an order of magnitude higher than previously reported results. The developed mechanical bonding technique may render various future experiments on novel materials, including high-T_c, and TI feasible, and our TI proximity demonstration paves the way for practical realization of TI-based devices involving superconductivity, including Majorana fermion based topological quantum computing.

The work at Rutgers was supported by National Science Foundation DMR-1104484. The work at the University of Toronto was supported by the Natural Sciences and Engineering Research Council of Canada, the Canadian Foundation for Innovation, and the Ontario Ministry for Innovation.

References and Notes:

1. P. Coleman, A. J. Schofield (2005). "Quantum criticality". Nature **433, 226** (2005).
2. P. A. Lee, N. Nagaosa, and X.-G. Wen, "Doping a Mott Insulator: Physics of High Temperature Superconductivity", Rev. Mod. Phys. 78, 17 (2006).
3. H. Deng, G. Weihs, C. Santori, J. Bloch, and Y. Yamamoto, "Condensation of Semiconductor Microcavity Exciton Polaritons," Science 298, 199 (2002).
4. L. Fu, C. L. Kane, and E. J. Mele, "Topological Insulators in Three Dimensions", Phys. Rev. Lett. **98**, 106803 (2007).
5. B. A. Bernevig, T. L. Hughes, S.-C. Zhang, "Quantum Spin Hall Effect and Topological Phase Transition in HgTe Quantum Wells", Science 314, 1757 (2006).
6. J. E. Moore and L. Balents, "Topological invariants of time-reversal-invariant band structures", Phys. Rev. B 75, 121306(R) (2007).
7. D. Hsieh, Y. Xia, L. Wray, D. Qian, A. Pal, J. H. Dil, J. Osterwalder, F. Meier, G. Bihlmayer, C. L. Kane, Y. S. Hor, R. J. Cava, and M. Z. Hasan, "Observation of Unconventional Quantum Spin Textures in Topological Insulators", Science **323**, 919 (2009).
8. Y. L. Chen, J. G. Analytis, J.-H. Chu, Z. K. Liu, S.-K. Mo, X. L. Qi, H. J. Zhang, D. H. Lu, X. Dai, Z. Fang, S. C. Zhang, I. R. Fisher, Z. Hussain, and Z.-X. Shen, "Experimental Realization of a Three-Dimensional Topological Insulator, Bi_2Te_3", Science **325**, 178 (2009).
9. X.-L. Qi, R. Li, J. Zang and S.-C. Zhang, "Inducing a Magnetic Monopole with Topological Surface States", Science **323**, 5918 (2009).

10. A. A. Burkov and D. G. Hawthorn, “Spin and charge transport on the surface of a topological insulator”, Phys. Rev. Lett. **105**, 066802 (2010).

11. S. A. Wolf, D. D. Awschalom, R. A. Buhrman, J. M. Daughton, S. von Molnár, M. L. Roukes, A. Y. Chtchelkanova and D. M. Treger, “Spintronics: A Spin-Based Electronics Vision for the Future”, Science **294**, 1488 (2001).

12. F. Wilczek,”Majorana returns”. Nature Phys. **5**, 614 (2009).

13. C. Nayak, S.H. Simon, A. Stern, M. Freedman, S. Das Sarma, “Non-Abelian anyons and topological quantum computation”. Rev. Mod. Phys. **80**, 1083 (2008).

14. A. Kitaev, “Fault-tolerant quantum computation by anyons”, Ann. Phys. (N.Y.) **303**, 2 (2003).

15. L. Fu and C. L. Kane, “Superconducting Proximity Effect and Majorana Fermions at the Surface of a Topological Insulator”, Phys. Rev. Lett. **100**, 096407 (2008).

16. H. B. Heersche, P. Jarillo-Herrero, J. B. Oostinga, L. M. K. Vandersypen, A. F. Morpurgo, “Bipolar supercurrent in graphene”, Nature **446,** 56 (2007).

17. H. Sasakura, S. Kuramitsu, Y. Hayashi, K. Tanaka, T. Akazaki, E. Hanamura, R. Inoue, H. Takayanagi, Y. Asano, C. Hermannstadter, H. Kumano, and I. Suemune, “Enhanced photon generation in a Nb/n-InGaAs/p-InP superconductor/semiconductor-diode light emitting device”, Phys. Rev. Lett. **107**, 157403 (2011).

18. I. Bozovic, G. Logvenov, M. A. J. Verhoeven, P. Caputo, E. Goldobin, and M. R. Beasley, “Giant proximity effect in cuprate superconductors”,Phys. Rev. Lett. **93**, 157002 (2004)

19. G. E. Blonder, M. Tinkham, and T. M. Klapwijk, "Transition from metallic to tunneling regimes in superconducting microconstrictions: Excess current, charge imbalance, and supercurrent conversion", Phys. Rev. B **25**, 4515 (1982).

20. P. C. van Son, H. van Kempen, and P. Wyder, "New method to study the proximity effect at the normal-metal–superconductor interface", Phys. Rev. Lett. **59**, 2226 (1987).

21. D. R. Heslinga, S. E. Shafranjuk, H. van Kempen, and T. M. Klapwijk, "Observation of double-gap-edge Andreev reflection at Si/Nb interfaces by point-contact spectroscopy", Phys. Rev. B **49**, 10484 (1994).

22. L. A. Wray, S.-Y. Xu, Y. Xia, Y. S. Hor, D. Qian, A. V. Fedorov, H. Lin, A. Bansil, R. J. Cava and M. Z. Hasan, "Observation of topological order in a superconducting doped topological insulator", Nature Phys., **6**, 855 (2010).

23. M. Kriener, K. Segawa, Z. Ren, S. Sasaki, and Y. Ando, "Bulk Superconducting Phase with a Full Energy Gap in the Doped Topological Insulator $Cu_xBi_2Se_3$", Phys. Rev. Lett. **106**, 127004 (2011).

24. S. Sasaki, M. Kriener, K. Segawa, K. Yada, Y. Tanaka, M. Sato, and Y. Ando "Topological superconductivity in $Cu_xBi_2Se_3$", to appear in Phys. Rev. Lett. (2011).

25. D. Zhang, J. Wang, A. M. DaSilva, J. S. Lee, H. R. Gutierrez, M. H. W. Chan, J. Jain, and N. Samarth, "Superconducting proximity effect and possible evidence for Pearl vortices in a candidate topological insulator", Phys. Rev. B **84**, 165120 (2011).

26. B. Sacepe, J.B. Oostinga, J. Li, A. Ubaldini, N.J.G. Couto, E. Giannini, A.F. Morpurgo, "Gate-tuned normal and superconducting transport at the surface of a topological insulator", arXiv:1101.2352v1 (2011).

27. Materials and methods are available as supporting material.

28. B. Pannetier and H. Courtois," Andreev Reflection and Proximity effect" J. Low Temp. Phys. **118**, 599. (2000).

29. S. Kashiwaya,Y. Tanaka, M. Koyanagi and K. Kajimura, "Theory for tunneling spectroscopy of anisotropic superconductors", Phys. Rev. B **53**, 2667 (1996).

30. Ch. Renner and Ø. Fischer, "Vacuum tunneling spectroscopy and asymmetric density of states of $Bi_2Sr_2CaCu_2O_{8+\delta}$", Phys. Rev. B **53**, 2667 (1996).

Figure captions:

Figure 1. **(A)** Atomic force microscope image of the crystal surface. **(B)** FIR spectrum of the Bi_2Se_3 crystal showing the plasma resonance corresponding to carrier density of 1.6×10^{19} cm^{-3}. **(C-F)** Junction fabrication technique : **(C)** Bi-2212 crystal is cleaved using scotch tape**. (D)** Bi_2Se_3 is sandwiched between glass slides with double-sided tapes and the top glass slide is lifted off, cleaving a flat surface. **(E)** Bi_2Se_3 transferred to a Cu sample holder, and the cleaved Bi-2212 crystal is applied to Bi_2Se_3 using GE varnish. **(F)** Contacts are made with Ag epoxy. **(G)** Experimental setup: four-point DC current-voltage and AC differential conductance measurements performed down to 4.5K, using a liquid He flow cryostat with lock-in amplifiers. DC bias from the power supply is combined with the AC signal from the voltage lock-in amplifier in a transformer-based adder.

Figure 2. **(A)** DC current-voltage characteristics of the low-resistance junction for different temperatures above and below T_c. Below T_c, excess current typical of Andreev reflection at an S-N interface is exhibited. 70K I-V curve shows the maximal excess current $I_e \sim 4.85\mu A$ – similar to the value of the normal junction (above T_c) at the voltage where the superconducting-state current becomes linear (black line). The total excess current is smaller for lower temperatures with I-V data showing additional features. **(B)** AC Differential conductance $\left[dI/dV\right]_S$, normalized by the normal state conductance $\left[dI/dV\right]_N$ at 105K, for a low-resistance junction at different temperatures above and

below T_c. A zero-bias conductance Andreev peak is clearly seen below T_c , with additional features in the spectrum appearing at lower temperatures. The curves are shifted for clarity. **(C)** DC current-voltage characteristics of the low-resistance junction for different temperatures well below T_C. In addition to the excess current, the low-temperature curves exhibit two distinct plateaus corresponding to the dips in the differential conductance measured for AC bias. The black arrow shows the induced Bi_2Se_3 gap (Δ_i) with a current twice of that of the normal state at the same voltage (Fig. 2 A), and the red arrow indicates the reduced Bi-2212 gap (Δ_r), while the intrinsic Bi-2212 gap (Δ_0) is shown by purple arrows. Thus, the total excess current I_s~2.7μA is smaller for lower temperatures. The inset shows the DC and the AC differential conductance at 4.5K, indicating the good correspondence between the different measurements of Δ_0 (purple arrow), Δ_r, and Δ_i (red arrow). **(D)** AC Differential conductance $\left[dI/dV\right]_S$, normalized by the normal state conductance $\left[dI/dV\right]_N$ at 105K, for a low-resistance junction for different temperatures well below T_C. The curves are shifted for clarity. The zero-bias conductance feature is due to the Andreev reflection between the normal and proximity induced superconducting regions in Bi_2Se_3, where the width of the peak is nearly $2\Delta_i$. The two additional peaks indicate the reduced and the intrinsic Bi-2212 gaps.

Figure 3. **(A)** A schematic drawing of the device in two regimes: (I) low-resistance with proximity induced superconductivity in Bi_2Se_3. Andreev scattering takes place in the whole proximity region with lower energy particles reflected mainly in Bi_2Se_3, and higher

energy ones mainly in Bi-2212. (II) High-resistance with no proximity induced superconductivity in Bi_2Se_3. Andreev scattering occurs at the interface. **(B)** Temperature dependence of the zero-bias differential conductance. Below T_c the Andreev process enhances the conductance by almost a factor of 2. The inset shows the temperature dependence of the reduced Bi-2212 gap Δ_i (blue circles) and the intrinsic Bi-2212 gap Δ_0 in the low-resistance junction (green squares), and in the high-resistance junction (red diamonds). **(C)** Differential conductance $[dI/dV]_S$, normalized by the normal state conductance $[dI/dV]_N$ at 105K, for a high-resistance junction for different temperatures, demonstrating the typical quasiparticle tunneling differential conductance resulting in a conductance dip in the gapped region. The curves are shifted for clarity. The red arrows indicate the intrinsic superconducting gap of Bi-2212 $\pm\Delta_0$ around 45mV.

Figure 1

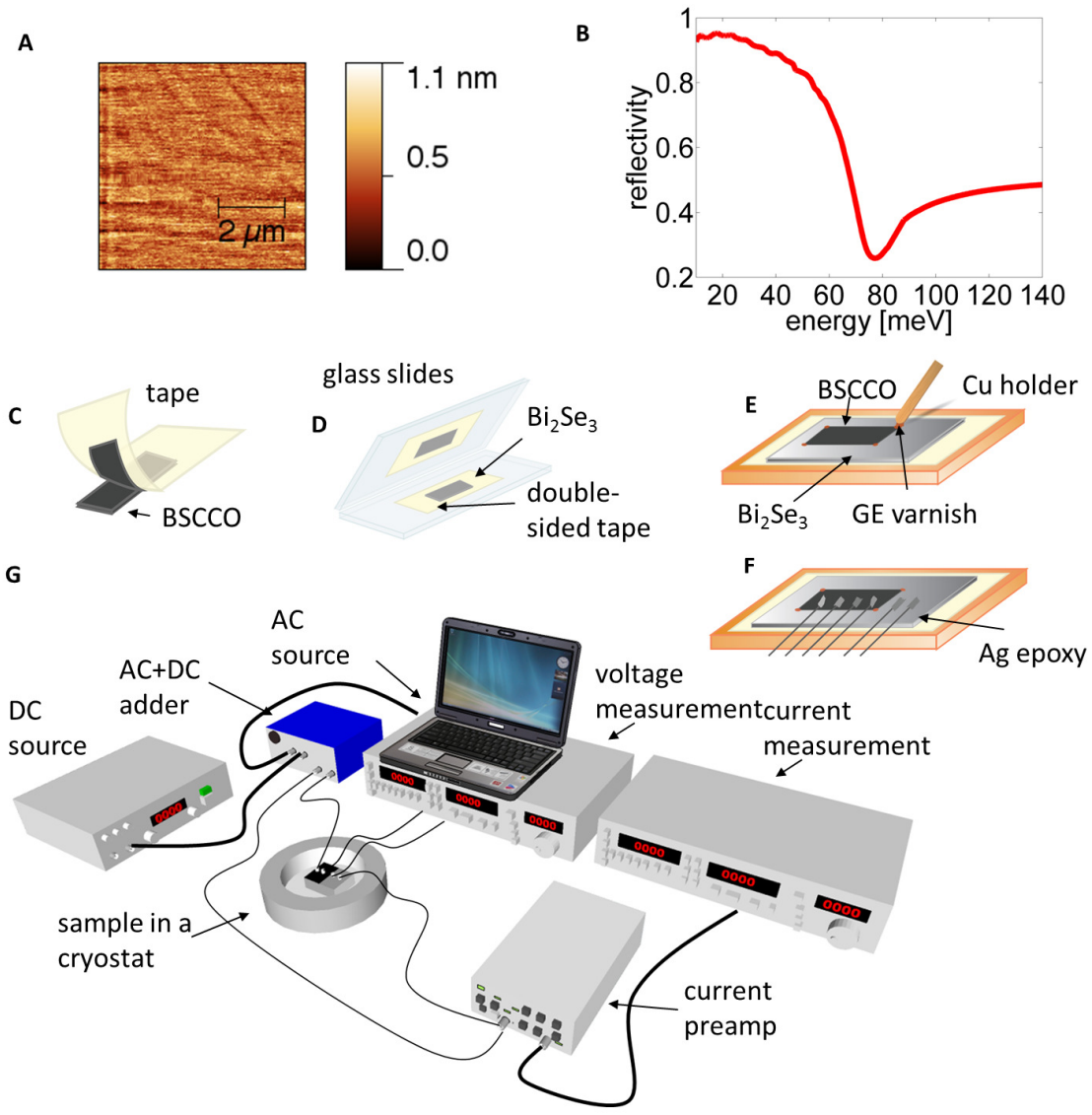
A
1.1 nm
0.5
0.0
2 μm
B
reflectivity
1
0.8
0.6
0.4
0.2
20 40 60 80 100 120 140
energy [meV]
C
tape
BSCCO
D
glass slides
Bi2Se3
double-
sided tape
E
BSCCO
Cu holder
Bi2Se3
GE varnish
F
Ag epoxy
G
AC
source
AC+DC
adder
DC
source
voltage
measurement
current
measurement
sample in a
cryostat
current
preamp

Figure 2

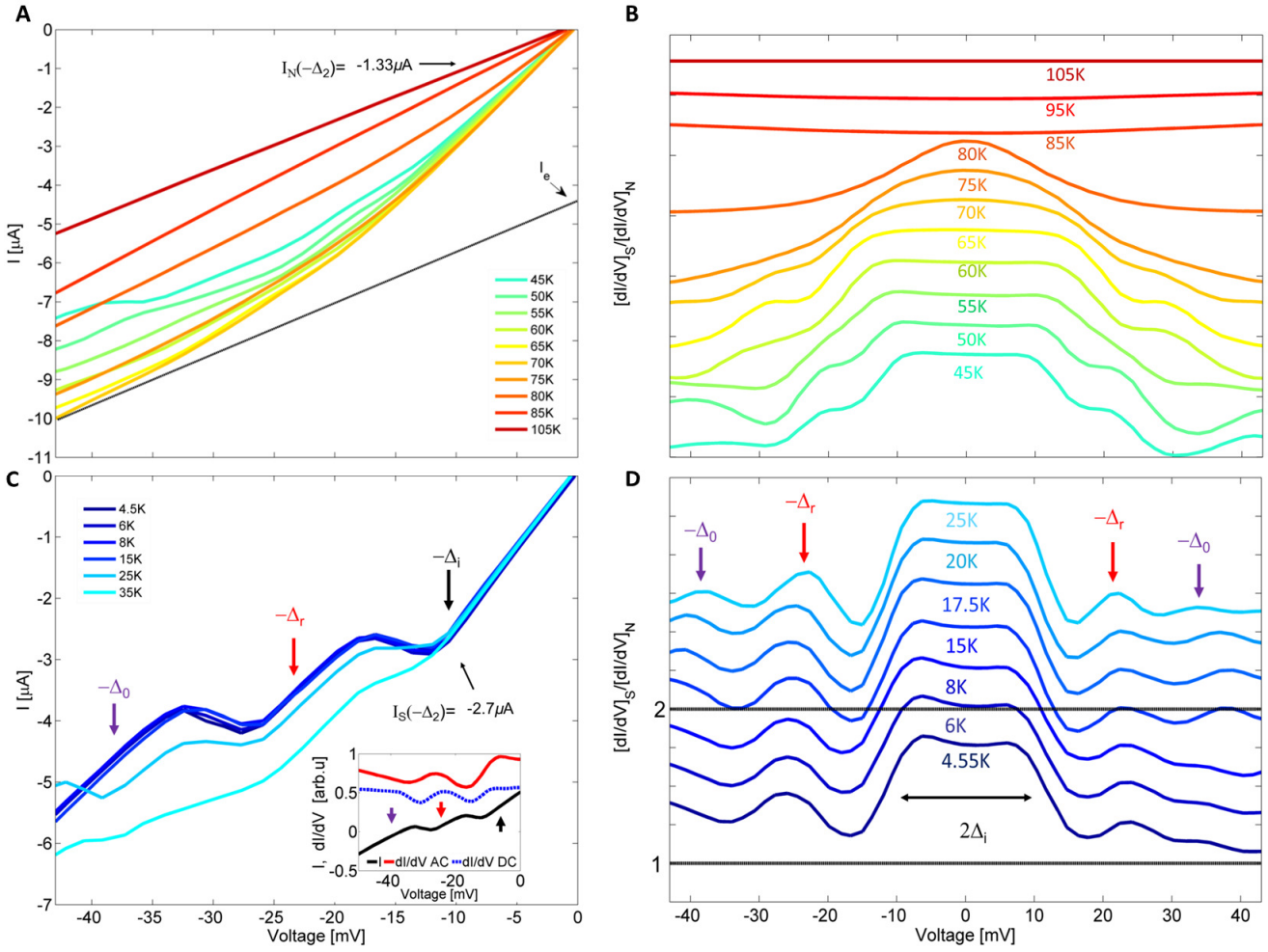
A
B
C
D
$I_N(-\Delta_2)$= -1.33μA
I_e
I [μA]
45K
50K
55K
60K
65K
70K
75K
80K
85K
105K
$[dI/dV]_S/[dI/dV]_N$
4.5K
6K
8K
15K
25K
35K
$-\Delta_i$
$-\Delta_r$
$-\Delta_0$
$I_S(-\Delta_2)$= -2.7μA
I, dI/dV [arb.u]
I
dI/dV AC
dI/dV DC
Voltage [mV]
$2\Delta_i$

Figure 3

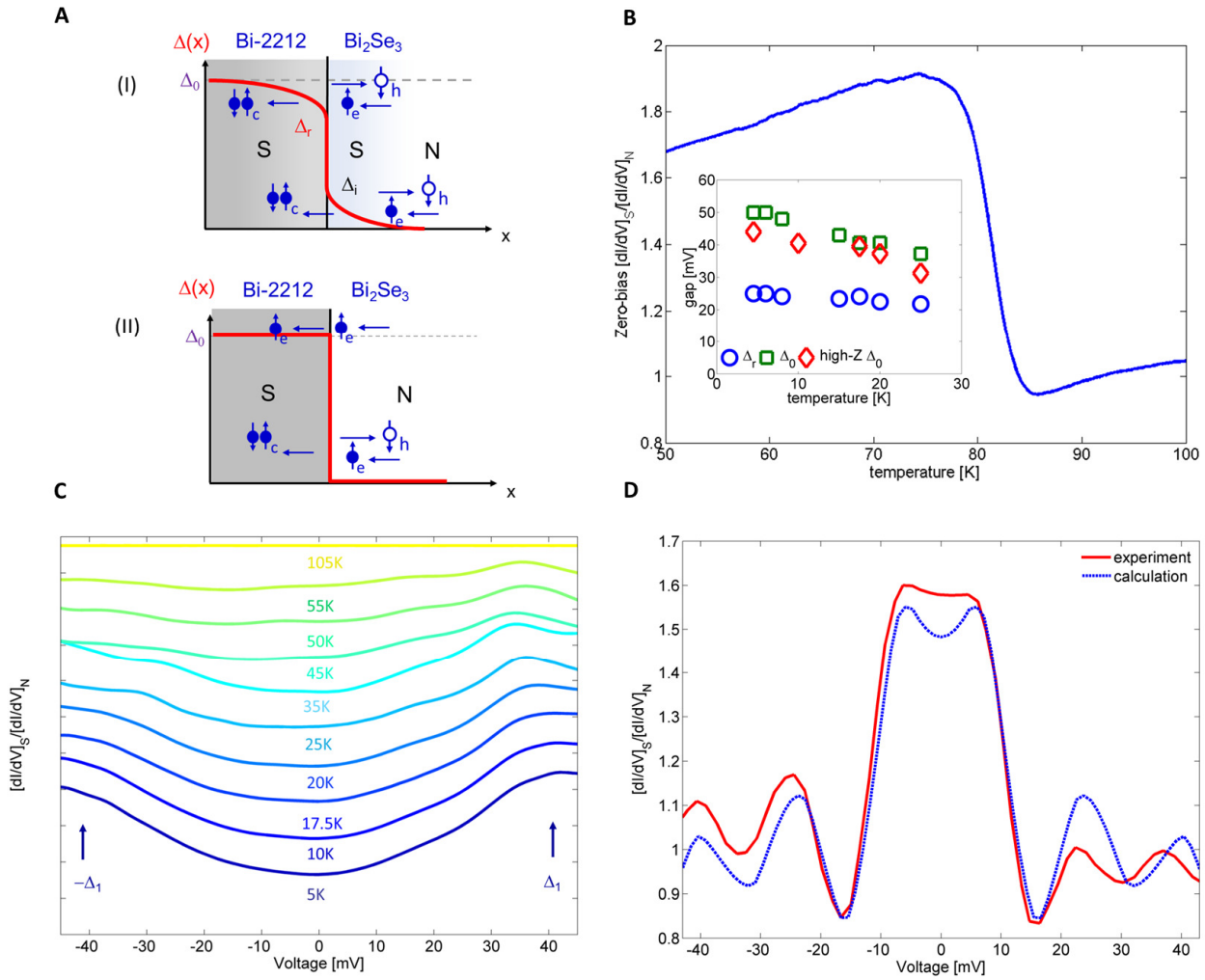
A
Δ(x)
Bi-2212
Bi2Se3
(I)
Δ0
Δr
Δi
S
S
N
x
(II)
B
Zero-bias [dI/dV]S/[dI/dV]N
temperature [K]
gap [mV]
Δr Δ0 high-Z Δ0
C
105K
55K
50K
45K
35K
25K
20K
17.5K
10K
5K
−Δ1
Δ1
[dI/dV]S/[dI/dV]N
Voltage [mV]
D
experiment
calculation
[dI/dV]S/[dI/dV]N
Voltage [mV]

Supporting Online Material for

High-temperature superconductivity in a topological insulator

Parisa Zareapour[1*], Alex Hayat[1,2*], Shu Yang F. Zhao[1], Anjan Reijnders[1], Mikhail Kreshchuk[1], Achint Jain[1], Daniel C. Kwok[3], Nara Lee[3], Sang-Wook Cheong[3], Zhijun Xu[4], Alina Yang[4], G. D. Gu[4], and Kenneth S. Burch[1]

[1]*Department of Physics and Institute for Optical Sciences, University of Toronto, 60 St. George Street, Toronto ON, M5S 1A7, Canada*

[2]*Centre for Quantum Information and Quantum Control University of Toronto, 60 St. George Street, Toronto ON, M5S 1A7, Canada*

[3]*Rutgers Center for Emergent Materials and Department of Physics and Astronomy, Rutgers University, 136 Frelinghuysen Road, Piscataway, New Jersey 08854, USA*

[4]*CMP&MS Department, Brookhaven National Laboratory, Upton, New York 11973, USA*

Device Fabrication: High-quality bulk Bi_2Se_3 crystals were prepared as described elsewhere *(S1)*. Additionally, optimally doped $Bi_2Sr_2CaCu_2O_{8+\delta}$ (Bi-2212) crystals ($T_C \approx 85K$) were grown by the floating-zone method *(S2)*. The carrier density of Bi_2Se_3 was determined by far infrared (FIR) spectroscopy. Specifically, reflectance of the (111) surface of the Bi_2Se_3 crystal was measured using a modified Bruker Vertex 80V FTIR spectrometer. The sample was mounted on a cone and gold coated in-situ to correct for spurious effects and produce absolute reflectance spectra (Fig. 1 B) *(S3)*. Comparison of the plasma edge at 78 meV with previous Bi_2Se_3 FIR spectroscopy data *(S4)* reveals a carrier density of $1.6 \cdot 10^{19}$ cm^{-3}. Bi-2212/Bi_2Se_3 tunnel junctions were fabricated by using

these crystals as the starting materials. Bi-2212 was cleaved in a dry box with adhesive tape (Fig 1. C), and a clean flat piece of Bi-2212 with the thickness of a few hundred μm was produced. Simultaneously Bi_2Se_3 was cleaved in the dry box by being sandwiched between two glass slides with double-sided tapes on both of them. After applying slight pressure to the glass slides, the top glass slide was lifted off (Fig 1. D). This approach was taken due to the difficulty of producing flat surfaces by cleaving Bi_2Se_3 with scotch tape, as was done for Bi-2212. Next, the Bi_2Se_3 was transferred to a Cu sample holder by attaching a double-sided tape to the Cu and placing one of the glass slides with Bi_2Se_3 on it on the sample holder. By lifting off the glass slide, a smooth and fresh surface of Bi_2Se_3 was left on the sample holder. The Bi-2212 was then attached to the Bi_2Se_3 by placing the Bi-2212 on the Bi_2Se_3, applying GE varnish on the corners of Bi-2212 (Fig 1. E). Contacts were made on the sample using Cu wires and Ag epoxy (Fig 1. F).

AC and DC Measurements Setup Description: Four-point probe measurements were performed in a Liquid Helium flow cryostat at different temperatures ranging from 295K to 4.5K. Bias-dependent differential conductance as well as current vs. voltage were measured on the Bi-2212/Bi_2Se_3 junction using two lock-in amplifiers (Stanford Research Systems SR810) with a resolution of 8mV, a DC voltage source (BK Precision 1787B), two DC multimeters (Hewlett Packard 3457A & Agilent 34401A) and a home-built, shielded AC+DC adder box (Fig 1.G). One of the lock-in amplifiers was used to produce a small AC voltage output at a frequency of 1.49 KHz. The AC voltage was added to the DC output of a DC power supply using a transformer-based adder. A voltage was applied

to the sample, with the resulting voltage measured with a lock-in (the AC part) and a multimeter (the DC part). At the same time, the current was converted to voltage and amplified with a current preamplifier (SRS 570) and measured with another lock-in (AC) and a multimeter (DC). Therefore, the AC current of the sample divided by the AC voltage of the sample, which is proportional to the dI/dV (differential conductance), was measured at different bias voltages.

A Bi-2212/Graphite mechanically-bonded junction was fabricated by the method described above, and AC differential conductance measurements were performed similar to the measurements done on Bi-2212/Bi_2Se_3. The graphite-based junction tunneling spectrum measurements show the typical high-resistance superconducting gap (Fig. S1) with the value of $\pm\Delta_1$ around 45mV – similar to those measured for Bi-2212/Bi_2Se_3.

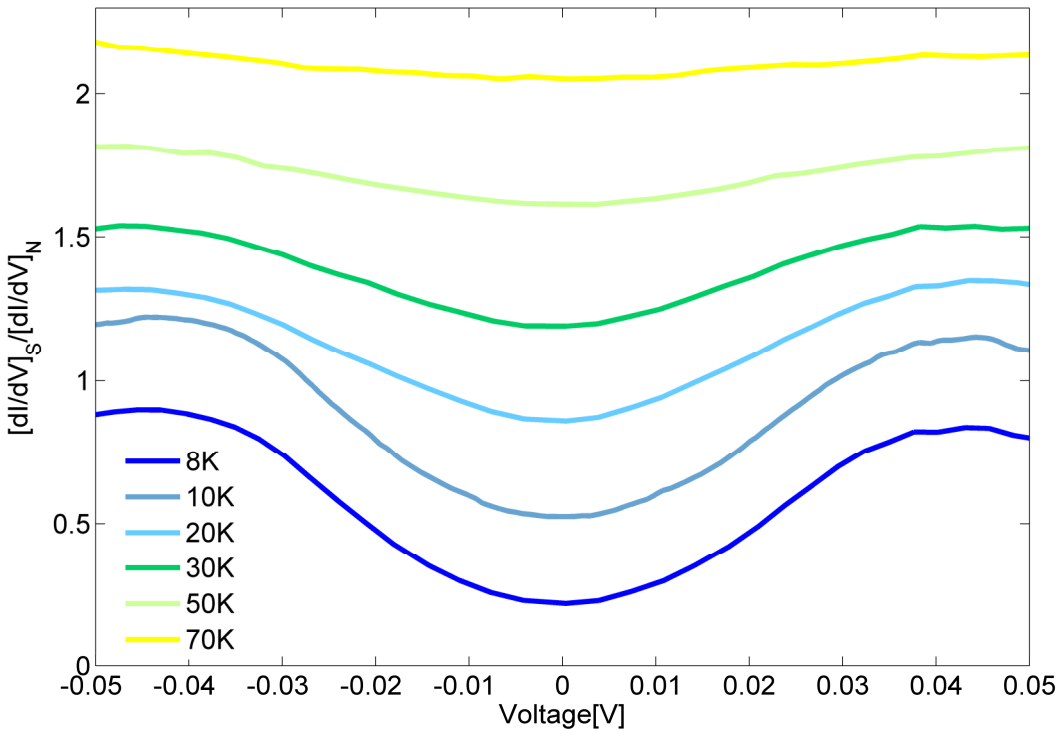

Figure S1. AC Differential conductance $\left[dI/dV\right]_S$ normalized by the normal state conductance $\left[dI/dV\right]_N$ at 105K for a Bi-2212/graphite junction at different temperatures below T_C. The curves are shifted for clarity.

SOM References:

S1. J. G. Analytis, J.-H. Chu, Y. Chen, F. Corredor, R. D. McDonald, Z. X. Shen, I. R. Fisher, "Bulk Fermi surface coexistence with Dirac surface state in Bi_2Se_3: A comparison of photoemission and Shubnikov–de Haas measurements", Phys. Rev. B, **81**, 205407 (2010).

S2. X. F. Sun, S. Ono, X. Zhao, Z. Q. Pang, Y. Abe, and Y. Ando, "Doping dependence of phonon and quasiparticle heat transport of pure and Dy-doped $Bi_2Sr_2CaCu_2O_{8+\delta}$ single crystals", Phys. Rev. B **77**, 094515 (2008) .

S3. C. C. Homes, M. Reedyk, D. A. Cradles and T. Timusk, "Technique for measuring the reflectance of irregular, submillimeter-sized samples". Appl. Opt., **32**, 2976 (1993).

S4. L. Tichý and J. Horák, "Nonparabolicity of the conduction band and anisotropy of the electron effective mass in n-Bi_2Se_3 single crystals", Phys. Rev. B **19**, 1126–1131 (1979).